Residual stress measurement in Fused Deposition Modelling parts

Residual stress measurement in Fused Deposition Modelling parts

Caterina Casavola[a], Alberto Cazzato[a], Vincenzo Moramarco[a,*] and Giovanni Pappalettera[a]

[a]Dipartimento di Meccanica, Matematica e Management (DMMM) - Politecnico di Bari - Viale Japigia 182 - 70126 Bari (Italy)

*phone +39 080 596 2830; fax +39 080 596 2777; e-mail vincenzo.moramarco@poliba.it

Abstract

The Fused Deposition Modelling (FDM), has become one of the most employed technologies to build complex 3D prototypes directly from a computerized solid model. In this process, the model is built as a layer-by-layer deposition of a feedstock wire. One of the most important issues in the FDM process is the distortion of the part during the print. This issue is due to the rapid heating and cooling cycles of the feedstock material that could produce accumulation of residual stresses during part building up. The aim of this work is to measure the residual stress in FDM parts made of ABS employing the hole-drilling method. In order to avoid the local reinforcement of the strain gage, an optical technique, i.e. ESPI (electronic speckle pattern interferometry), is employed to measure the displacement of the surface due to the stress relaxation. Furthermore, the effect of the stacking sequences and the residual stress distribution on each side of the specimen have been investigated.

Keywords: Fused Deposition Modelling; hole drilling; Electronic Speckle Pattern Interferometry; residual stresses; orthotropic materials.

1. Introduction

The Fused Deposition Modelling (FDM), invented in the early 1990s by Stratasys, has become one of the most employed technologies to build complex 3D prototypes directly from a computerized solid model. Nowadays, this technology is used in many fields such as aerospace, medical, construction, cultural [1, 2] but there are many other potential fields where it could be employed. Moreover, the diffusion of the low-cost desktop 3D printers such as RepRap, Maker-Bot, Cube, etc., has made this technology widely accessible even at home and office.

In this process, as for many others 3D printing technologies [3], the model is built as a layer-by-layer deposition of a feedstock material. Initially, this is in the form of filament that is, successively, partially melted, extruded and deposited by a numerically guided heated nozzle onto the previously built model [1]. After the deposition,

the material cools, solidifies and sticks with the surrounding material. Once the entire model has been deposited, the FDM part shows orthotropic material properties with a behaviour similar to a laminate orthotropic structure [4, 5]. Nowadays, besides the traditional FDM materials such as PLA (polylactic acid) and ABS (acrilonitrile-butadiene-stirene), many others materials have been employed and developed, e.g., short fibre composites [6], metals [7], bioresorbable polymers (PCL) [8], ceramics [9] and metal/polymers mixture materials [10]. The PLA has better thermo-mechanical characteristics than ABS showing a higher mechanical resistance and a lower coefficient of thermal expansion that improves the printability of PLA reducing the warp effect during the printing phase. Indeed, the distortion of the part during the print is one of the most important issues in the FDM process. The rapid heating and cooling cycles of the feedstock material could produce accumulation of residual stresses during part building up [11, 12]. This residual stress could lead to distortion and de-layering problems [13], which seriously affect the shape and the final dimensions of the parts or it could prevent the finalization of the objects due to unsticking of the part from the bed. In order to reduce these issues, a common technique is to use a heated bed with some type of adhesive on the surface of the bed. Although, such procedures help to reduce distortions, they can increase the residual stresses in the final part.

Several techniques can be employed to measure the residual stress in plastic parts. One of the most well-known is the incremental hole-drilling method [14]. In this semi-destructive technique, the introduction of a hole into a stressed body causes localized stress relaxation and deformation around the hole. The strain distribution can be measured by a strain gage rosette or by an optical technique [15]. Until now, some works have dealt with experimental measurements to determine residual stress distribution in plastic parts [16-19] but, to the authors' knowledge, no one in FDM parts. Turnbull et al. [16] carried out a comparison among several techniques in order to measure residual stresses in polymers such as Polycarbonate, ABS and Nylon. They concluded that the hole drilling is in accordance with the other techniques and, even if it shows some problems due to the calculation procedures, it can be employed as a valid measurement method. Nau et al. [17] highlighted that the procedures and process parameters valid for stress analysis in metallic materials cannot be applied in plastic materials. They pointed out that the surface preparation of specimens, the strain gauge bonding and the drilling speed are critical issues in order to obtain a correct measure. However, both Turnbull et al. [16] and Nau et al. [17] did not consider the local reinforcement effect that the installation of a rosette produces in materials that

have a low Young's modulus. Finally, Magnier et al. [15] carried out a deep investigation on the influence of material viscoelasticity, room temperature and local reinforcement of the strain gauge on the measure of deformation by HDM of plastic materials. They pointed out how these parameters can produce a difference up to 30% between the results recorded by strain gauge and DIC.

Only one paper has tried to deal with the residual stress issues in FDM by numerical simulation. Zhang and Chou [20], using simplified material properties and boundary conditions, have simulated different deposition patterns and have demonstrated the feasibility of using the element activation function to reproduce the filament deposition. They found that residual stress is higher in the first deposited layer compared to the last layer and that there was a modification of the residual stress distributions changing the tool-path pattern. However, they did not validate their model using residual stress measurements but only by comparing the distortion of the printed part and the numerical prediction.

The aim of this work is to measure the residual stress in FDM parts made of ABS employing the hole-drilling method. In order to avoid the local reinforcement of the strain gage, an optical technique, i.e. ESPI (electronic speckle pattern interferometry), is employed to measure the displacement of the surface due to the stress relaxation. Furthermore, the effect of the stacking sequences on the residual stress distribution has been investigated. Four stacking sequences have been printed, i.e. ±30°, ±45°, 0°/90° and 0° only. In addition, the residual stress distribution on each side of the specimen has been investigated; for this purpose the measurements have been carried out on the top, i.e. the last printed layer, and the bottom of the specimens, i.e. the first printed layer.

2. Materials and methods

In this work, the ESPI technique has been employed to measure the displacement around a hole drilled inside the material. Due to the orthotropic behaviour of FDM parts, the isotropic model usually implemented in commercial hole drilling software cannot be used. Thus, an orthotropic FEM model has been developed to calculate the displacements due to some known stress cases. The combination between the experimental displacement data and the FE model allows calculating the residual stress in the parts.

2.1. Experimental procedure

A RepRap Prusa i3 equipped with a marlin firmware and a nozzle with a diameter of 0.4 mm has been employed to produce the specimens. These have a rectangular shape and the dimensions of 80 x 40 x 7 mm.

Four stacking sequences have been studied, i.e., the raster angles are ±30°, ±45°, 0°/90° and 0° only. A layer with a 0° raster angle have the deposited beads parallel to the major side of the specimen. Moreover, the samples have been fabricated with the minimum dimension of the part perpendicular to the build platform. The Figure 1 shows the coordinate system for the deposition and for the residual stresses.

Figure 1 Specimen examples with ± 45° (a) and 0°/90° (b) stacking sequence

The parameters reported in Table 1, such as the layer thickness or the number of contour lines, have been kept constant for every specimen.

Table 1 Fixed printer parameters

Parameter	**Value**
Air gap [mm]	0
Layer thickness [mm]	0.2
Bead width [mm]	0.67
Number of contour lines	3
Bed temperature [°C]	90
Nozzle temperature [°C]	215

In Table 1, the air gap is the distance between two, adjacently deposited, beads of the same layer; the layer thickness and the bead width are respectively the height and the width of a deposited filament. The number of contours represents how many edges have been deposited before filling the inner part by inclined beads. The bed temperature has been set to 90 °C and some glue on the bed has been employed to reduce the warping effect. The solid model, created using a 3D CAD, has been sliced using the open source software Slic3r.

The measure of the residual stresses has been carried out on three different samples for each stacking sequence. Moreover, to obtain a better knowledge of the residual stress in the top and the bottom of the samples, three holes have been drilled on the top of each specimen, i.e. starting from the last layer deposited, and three on the bottom, i.e. starting from the first layer deposited (Figure 2). An average value for each side of the specimen has been calculated based on the data of these three holes.

Figure 2 Holes position on the top and the bottom of the specimens

The holes were drilled by means of a high-speed turbine which is mounted on a precision travel stage. Turbine rotation speed was set to 5000 rpm after some preliminary tests that indicated that this speed allows obtaining good quality holes [12]. The cutter is made by tungsten coated by TiN and it has a nominal diameter d =1.59 mm. Compressed air was activated during the test to clean the surface of the sample by the formation of drilling chips. The holes were drilled to a depth of 0.6 mm through 30 drill increments to contain the temperature

during the drilling phase on lower values. In order to reduce the computational time, the residual stress calculation has been done on 15 drill increments.

A diode pumped solid state laser source (λ=532 nm) was used to shine the sample and to generate the speckle pattern. The laser beam is divided in two parts by a beamsplitter and delivered by two optical fibres. The beam emerging out from the first fibre is collimated and then directed towards the sample at a given angle (α=54°). The beam emerging from the second fibre, instead, is directed towards the CCD matrix of the camera and acts as a reference beam. The CCD camera (640x480 pixel) itself is placed at a given angle with respect to the normal to the sample (β=34°). Light diffused by the sample interferes on the CCD matrix with the reference beam. Four-step temporal phase shifting algorithm was adopted in order to obtain the phase [21, 22]. This means that four reference images are taken initially having a $\pi/2$ phase difference among each other. Another set of four images is, analogously taken for each drill increment. These intensity patterns were subtracted from the reference intensity pattern recorded on the sample before starting the drilling procedure. This operation allows obtaining fringe patterns encoding the information about the displacement experienced by the sample along the sensitivity vector.

2.2. Residual stress calculation

In the present work, the integral method has been used to calculate the residual stresses. In the ESPI technique, a reference set of phase-stepped images of the specimen surface around the hole is acquired before the start of hole drilling and then after each incremental increase in hole depth. The images acquired after each increment in depth are correlated with the previous set to calculate the incremental displacements of the surface around the hole. The relationship between the measured incremental displacements **d** and the stresses **σ** within each step can be expressed as a matrix equation [23]:

$$\mathbf{D\sigma} = \mathbf{d} \tag{1}$$

where **D** is a matrix, **σ** and **d** are vectors. Matrix element D_{ij} represents the incremental surface displacements measured after hole depth increment i caused by a unit stress within increment j. For ESPI measurements, each camera pixel provides an information of the displacements and thus the vector **d** represents the n measured pixels around the drilled hole, where n is typically millions of pixels. Because of this excess of data, the equation (1) is overdetermined and can be solved by using a least square method:

$$\mathbf{D}^{\mathrm{T}}\mathbf{D\sigma} = \mathbf{D}^{\mathrm{T}}\mathbf{d} \tag{2}$$

The computation of the residual stress has been carried out calculating the matrix **D** using a finite element model, measuring the incremental displacements **d** and then solving the equation (2) to determine the stresses **σ**. In the residual stresses calculation, the rigid body motions of the sample due to the hole drilling have been opportunely taken into account.

The orthotropic behaviour of FDM parts requires the development of an orthotropic FEM model for each raster orientation case under study. The required **D** matrix has been calculated considering the actual values of the hole diameter, the depth of the hole and steps of the drilling procedure. A SOLID185 layered element has been employed to have the possibility to simulate the raster orientation of each layer. The mechanical properties of the single layers has been based on the data from a previous work made by Casavola et al. [4]. In Figure 3 the mesh structure of the model has been reported.

Figure 3 Finite element model mesh

For an easier meshing process and to reduce the computational time, only a cylindrical zone near the hole that has a radius of 8 times the radius of the hole has been modelled. In order to better follow the displacement field without increasing the computational time, the mesh is finer near the hole, where higher displacement was expected. For the same reason, the elements on the top of the model, for the entire drilling depth, have the same height of the calculation steps (i.e. 0.04 mm), while elements of the lower layers are thicker (i.e. 0.4 mm). Each step of hole-drilling process has been simulated, using a birth and dead technique, by removing elements at the hole area, applying loads on the elements forming wall of the drilled hole, and then calculating the corresponding displacements around the hole. This procedure has been repeated until the whole hole has been simulated. For each depth increment, three load cases have been considered: $\sigma_x = 1\ MPa$, $\sigma_y = 1\ MPa$ and $\tau_{xy} = 1\ MPa$. To apply each of these loads, the equivalent radial and hoop stress distributions were applied simultaneously to the hole face according to Akbari et al. [24].

3. Results and Discussion

Due to the low melting point of the ABS, the effects of the local increase of temperature due to drilling speed should be considered. As reported in Casavola et al. [12], the drilling speed has been set to 5000 rpm after some preliminary tests that have been summed up in Figure 4. In this Figure, the hole macrography and thermograms comparison between 5000 rpm (Figure 4a, Figure 4b) and 50000 rpm (Figure 4c, Figure 4d) have been reported.

Figure 4 Hole macrography and temperatures maps comparison between 5000 rpm (a, b) and 50000 rpm (c, d).

The temperatures comparison between Figure 4b and Figure 4d shows that increasing the drilling speed from 5000 to 50000 rpm leads to an increase of temperature from 31.9 °C to 77.9 °C. This could explain the difference in the hole quality between the two drilling speeds as reported in Figure 4a and Figure 4c. The hole bottom is flat and regular for the 5000 rpm drilling speed whereas, for 50000 rpm, there is a central bulge that is probably due to a local boiling of the ABS material during the drilling process.

In Figure 5 an example of fringe pattern for a 0/90° has been reported. These type of images, that have been obtained subtracting two intensity patterns in different drilling steps, encode the information about the displacements experienced by the sample along the sensitivity vector. Employing a four-step temporal phase shifting algorithm is possible to obtain the displacement maps near the drilled hole (Figure 6).

Figure 5 Example of fringe pattern for the sample 0/90°

Figure 6 Example of displacements maps in some stacking sequences

The Figure 7 and Figure 8 show the residual stresses trends, σ_x, σ_y and τ_{xy}, for the four stacking sequences. The residual stresses on each side of the specimen, i.e. top and bottom, are the average values calculated based on the data of the three drilled holes per side. In general, as can be point out in Figure 7, for σ_x and σ_y there are some differences among the stacking sequences analysed. These differences are remarkable near the surface of the specimens, i.e. until 0.2 mm, but after this depth, there are no clear differences between the configurations. The residual stresses for the ± 30° configuration (Figure 7b and Figure 7g), in absolute value, are higher than the other configurations both on the top and on the bottom of the specimens. Moreover, this stacking sequence shows the highest value of residual stress recorded during this experimental campaign (Figure 7g). Indeed, the σ_y residual stress on the bottom reaches a value 6 MPa near 0.3 mm of depth. Considering that the yielding point of ABS is 26 MPa, a value of 6 MPa is more than 20% of the yielding point of the material. The ± 45° should be the best configuration to have low residual stresses in the specimens. In the σ_x (Figure 7b) and τ_{xy} (Figure 8) directions, the residual stresses are near the zero on both the top and the bottom of the specimens. The σ_y (Figure 7f) direction shows values higher than the other two directions but, however, lower than the other configurations.

Figure 7 Residual stresses measured in σ_x and σ_y directions on the top and the bottom of the specimens

As it can be pointed out in Figure 8, for the τ_{xy} cannot be observed any significant difference among the stacking sequences and the side of the specimens. Indeed, the values of residual stress is roughly between -1 MPa and 1 MPa in all configurations.

Figure 8 Residual stresses measured in τ_{xy} direction on the top and the bottom of the specimens

Although the bottom of the FDM part that tend to warp during the printing phase and it has been constrained by the glue, there are no clear differences between the top and the bottom of the specimens in all configurations. Generally, for the σ_x direction, there are compression values near the surface of the specimens until the depth of 0.2 mm. After this value of depth, the specimens show low value of tensile residual stress in all configurations. A similar trend with lower value of residual stress near the surface and tensile stress in the inner part of the sample can be highlighted also for the σ_y. Although in this direction, the magnitude of the residual stress in the inner part of the specimen is higher than the σ_x direction.

4. Conclusions

In this paper, the measure of the residual stresses in FDM printed specimens has been carried out by the hole-drilling method. An optical technique, i.e. ESPI, has been employed to measure the displacements produced during the hole drilling procedure. This technique allows avoiding local reinforcement due to strain gauge rosette that is a serious issue in materials, such as ABS, that have a low Young's module. Furthermore, the effect of the stacking sequences on the residual stress distribution has been investigated. Four stacking sequences have been studied, i.e. ±30°, ±45°, 0°/90° and 0° only. Moreover, the residual stress distribution on each side of the specimen has been studied, measuring the stresses on the top and the bottom of the samples. The specimens have been made of ABS and they have the dimensions of 80 x 40 x 7 mm.

Some preliminary tests have been carried out to determine the optimal drilling parameters. These have highlighted that the local increase of temperature due to the drilling procedure can seriously influence the quality of the hole. The thermographic analysis show an increment of the temperature from 31.9 °C for 5000 rpm to 77.9 °C for 50000 rpm. This is confirmed by the macrographs that show a regular hole with a flat bottom for the lower drilling speed, whereas for the higher, there is a central bulge. This is probably due to a local boiling of the material during the process.

The results show that, whereas for τ_{xy} cannot be observed any difference among the stacking sequences as well as the sides of the specimens, for σ_x and σ_y there are some differences. These are remarkably near the surface

of the specimens, i.e. until 0.2 mm, but after this depth, there are no clear differences among the studied configurations. Whereas the ± 30° configuration is the worst stacking sequence because it shows the highest values of residual stresses, the ± 45° should be the best configuration to have low residual stresses in the specimens. Moreover, the comparison between the top and the bottom of the specimens shows no clear differences in all configurations. Finally, the highest value of residual stress recorded during this experimental campaign is 6 MPa and considering that the yielding point of ABS is 26 MPa, a value of 6 MPa is more than 20% of the yielding point of the material. This result confirms that residual stress management in FDM part is an important issue that must be properly addressed and taken into account in order to reduce warping effects and delayering problems in the finished part.

References

[1] X. Yan, P. Gu. A review of rapid prototyping technologies and systems. Comput Aided Design 1996;28:307-318.

[2] R. Petzold, H.F. Zeilhofer, W.A. Kalender. Rapid prototyping technology in medicine - basics and applications. Comput Med Imag Grap 1999;23:277-284.

[3] C.K. Chua, S.M. Chou, T.S. Wong. A study of the state-of-the-art rapid prototyping technologies. Int J Adv Manuf Technol 1998;14:146-152.

[4] C. Casavola, A. Cazzato, V. Moramarco, C. Pappalettere. Orthotropic mechanical properties of fused deposition modelling parts described by classical laminate theory. Mater Design 2016;90:453-458.

[5] W.C. Smith, R.W. Dean. Structural characteristics of fused deposition modeling polycarbonate material. Polym Test 2013;32:1306-1312.

[6] W. Zhong, F. Li, Z. Zhang, L. Song, Z. Li. Short fiber reinforced composites for fused deposition modelling. Mat Sci Eng A-Struct 2001;301:125-130.

[7] J. Mireles, H.-C. Kim, I. Hwan Lee, D. Espalin, F. Medina, E. MacDonald, R. Wicker. Development of a Fused Deposition Modeling System for Low Melting Temperature Metal Alloys. J Electron Packaging 2013;135.

[8] I. Zein, D.W. Hutmacher, K.C. Tan, S.H. Teoh. Fused deposition modeling of novel scaffold architectures for tissue engineering applications. Biomaterials 2002;23:1169-1185.

[9] M. Allahverdi, S.C. Danforth, M. Jafari, A. Safari. Processing of advanced electroceramic components by fused deposition technique. J Eur Ceram Soc 2001;21:1485-1490.

[10] S.H. Masood, W.Q. Song. Development of new metal/polymer materials for rapid tooling using Fused deposition modelling. Mater Design 2004;25:587-594.

[11] A. Kantaros, D. Karalekas. Fiber Bragg grating based investigation of residual strains in ABS parts fabricated by fused deposition modeling process. Mater Design 2013;50:44-50.

[12] C. Casavola, A. Cazzato, V. Moramarco, G. Pappalettera. Preliminary Study on Residual Stress in FDM Parts. Residual Stress, Thermomechanics & Infrared Imaging, Hybrid Techniques and Inverse Problems, Volume 9, Springer International Publishing 2017, pp. 91-96.

[13] S.N. Economidou, D. Karalekas. Optical sensor-based measurements of thermal expansion coefficient in additive manufacturing. Polym Test 2016;51:117-121.

[14] G.S. Schajer, P.S. Whitehead, Hole Drilling and Ring Coring. Practical Residual Stress Measurement Methods, John Wiley & Sons, Ltd 2013, pp. 29-64.

[15] D.V. Nelson, Optical Methods, Practical Residual Stress Measurement Methods, John Wiley & Sons, Ltd 2013, pp. 279-302.

[16] A. Turnbull, A.S. Maxwell, S. Pillai. Residual stress in polymers - evaluation of measurement techniques. J Mater Sci 1999;34:451-459.

[17] A. Nau, B. Scholtes, M. Rohleder, J. Nobre. Application of the hole drilling method for residual stress analyses in components made of polycarbonate. J Plast Tec 2011:66-85.

[18] A. Magnier, A. Nau, B. Scholtes. Some aspects of the application of the hole drilling method on plastic materials. Conference Proceedings of the Society for Experimental Mechanics Series, 2016, pp. 371-380.

[19] A.S. Maxwell, A. Turnbull. Measurement of residual stress in engineering plastics using the hole-drilling technique. Polym Test 2003;22:231-233.

[20] Y. Zhang, Y. Chou. Three-dimensional finite element analysis simulations of the fused deposition modelling process. P I Mech Eng B-J Eng 2006;220:1663-1671.

[21] M. Kujawinska. Use of phase-stepping automatic fringe analysis in moire interferometry. Appl Optics 1987;26:4712-4714.

[22] D.C. Ghiglia. M.D. Pritt, Two-dimensional phase unwrapping: theory, algorithms, and software, Wiley New York 1998.

[23] G.S. Schajer, T.J. Rickert, Incremental Computation Technique for Residual Stress Calculations Using the Integral Method, in: T. Proulx (Ed.) Experimental and Applied Mechanics, Volume 6: Proceedings of the 2010 Annual Conference on Experimental and Applied Mechanics, Springer New York, New York, NY, 2011, pp. 185-191.

[24] S. Akbari, F. Taheri-Behrooz, M.M. Shokrieh. Characterization of residual stresses in a thin-walled filament wound carbon/epoxy ring using incremental hole drilling method. Compos Sci Technol 2014;94:8-15.

Captions

Figure 1 Specimen examples with ± 45° (a) and 0°/90° (b) stacking sequence

Figure 2 Holes position on the top and the bottom of the specimens

Figure 3 Finite element model mesh

Figure 4 Hole macrography and temperatures maps comparison between 5000 rpm (a, b) and 50000 rpm (c, d).

Figure 5 Example of fringe pattern for the sample 0/90°

Figure 6 Example of displacements maps in some stacking sequences

Figure 7 Residual stresses measured in σ_x and σ_y directions on the top and the bottom of the specimens

Figure 8 Residual stresses measured in τ_{xy} direction on the top and the bottom of the specimens

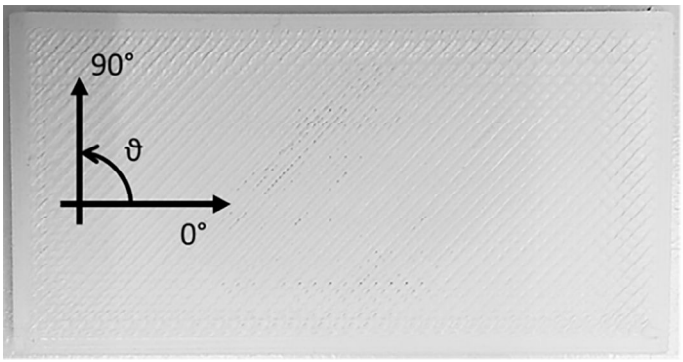

a

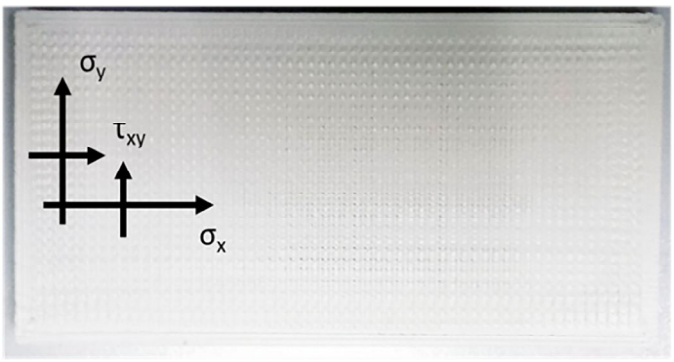

b

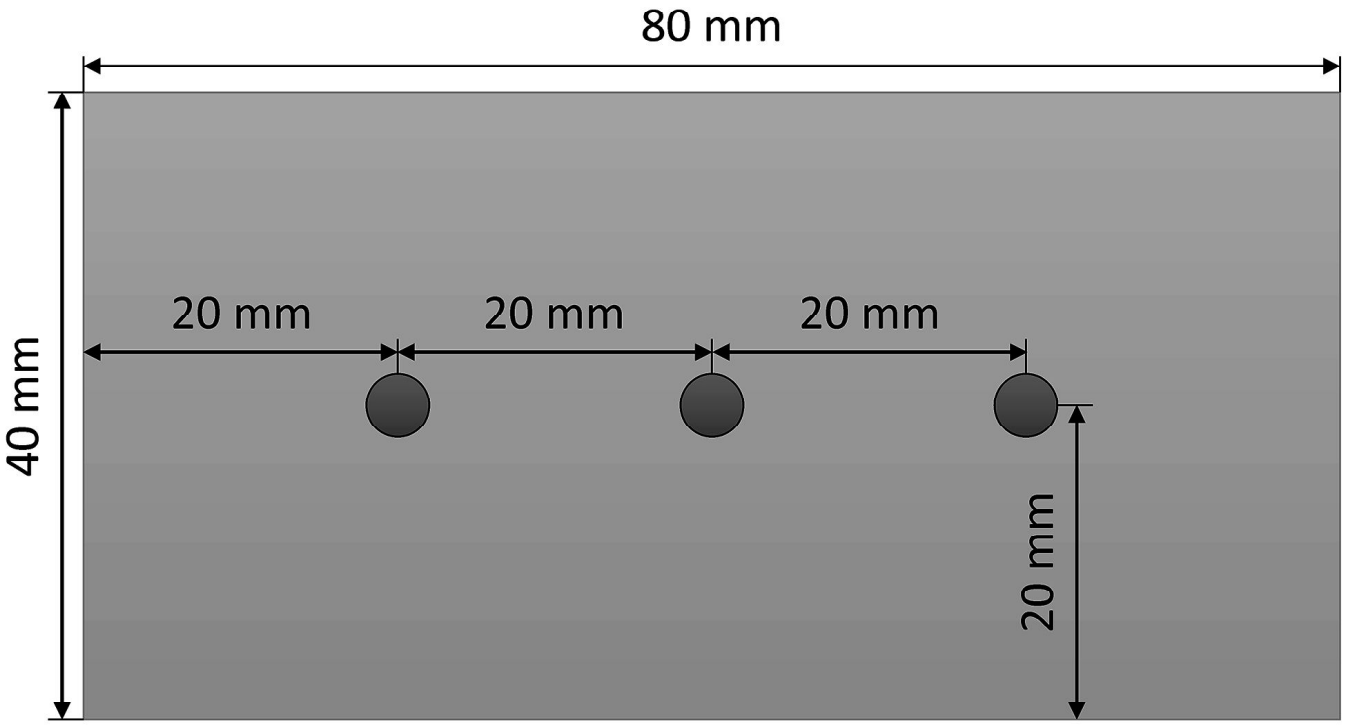
80 mm
40 mm
20 mm
20 mm
20 mm
20 mm

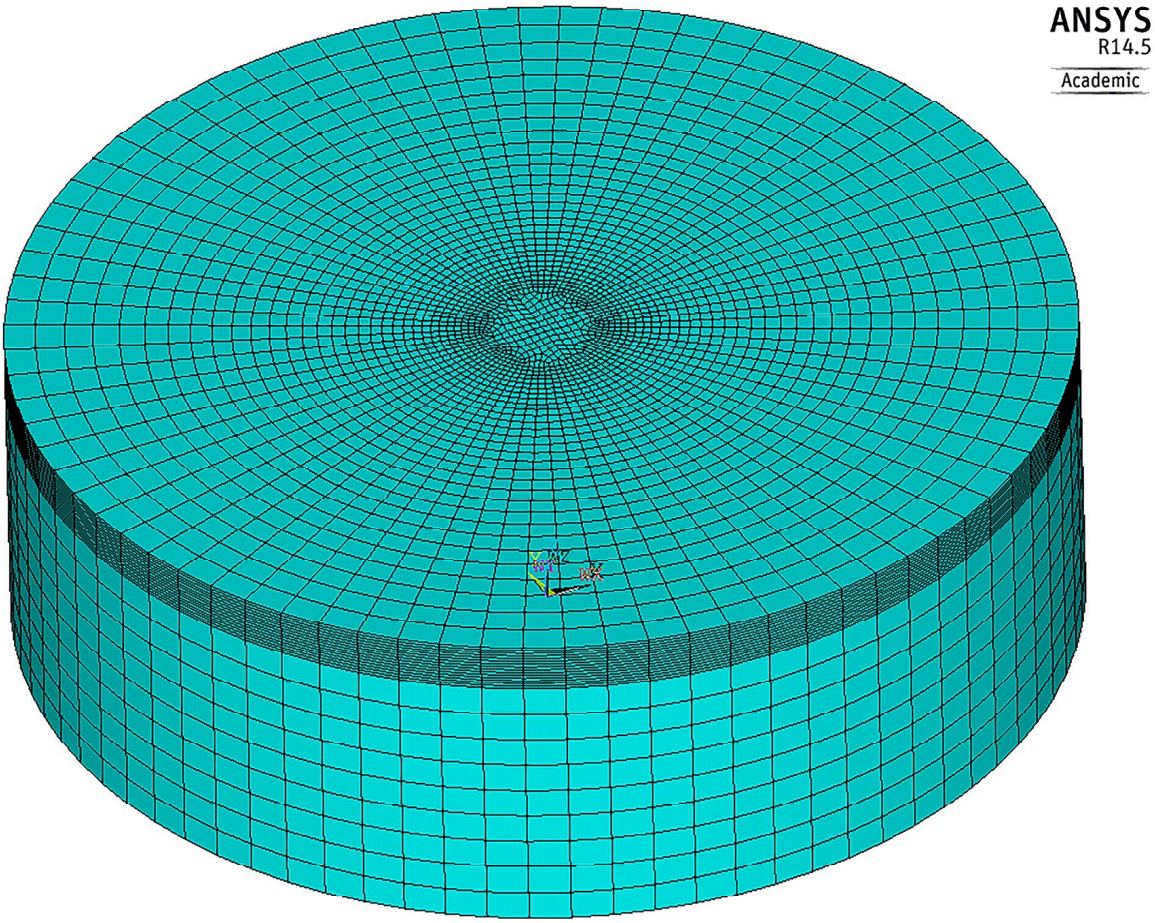
ANSYS
R14.5
Academic

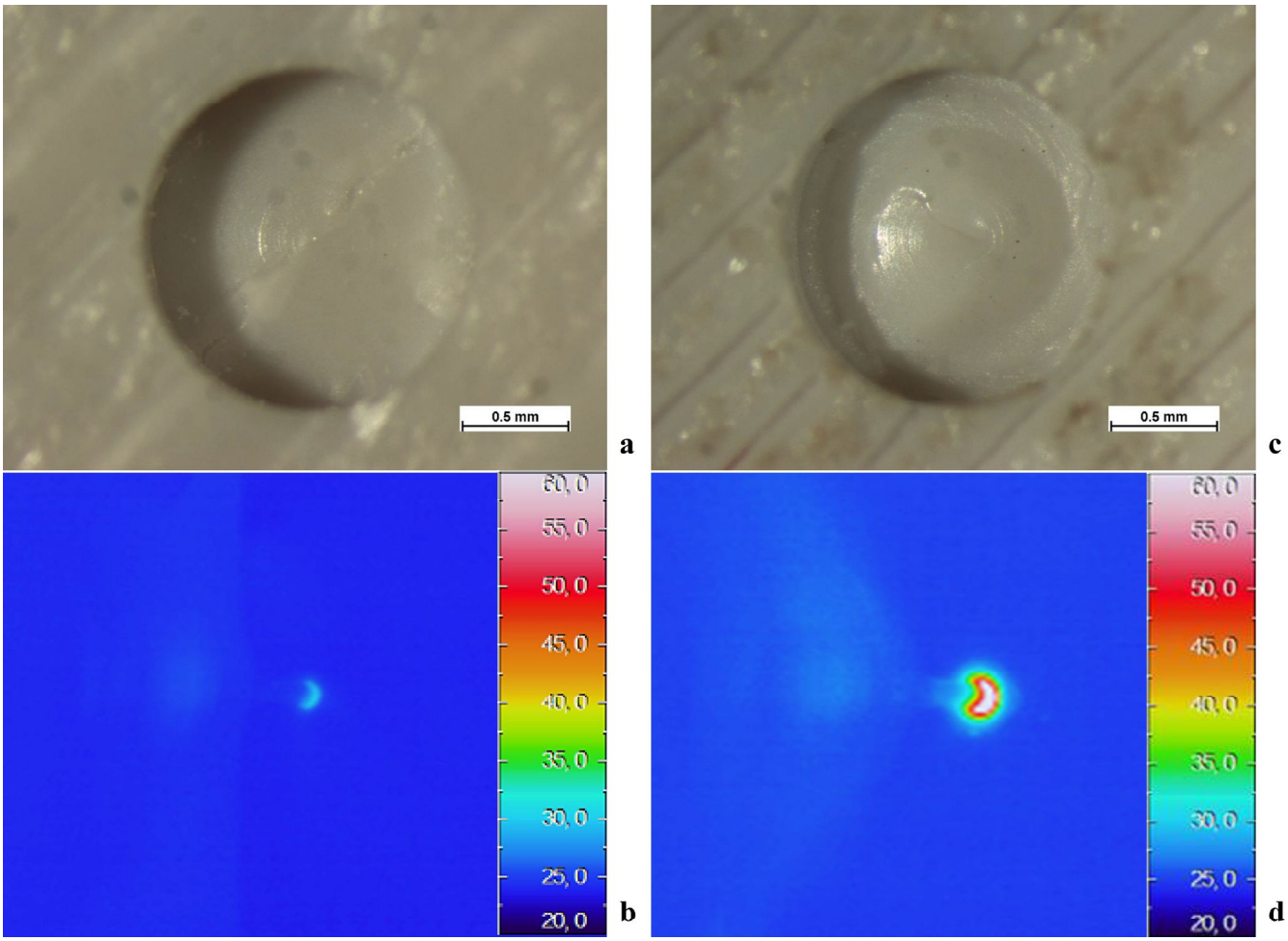
0.5 mm
a
0.5 mm
c
60, 0
55, 0
50, 0
45, 0
40, 0
35, 0
30, 0
25, 0
20, 0
b
60, 0
55, 0
50, 0
45, 0
40, 0
35, 0
30, 0
25, 0
20, 0
d

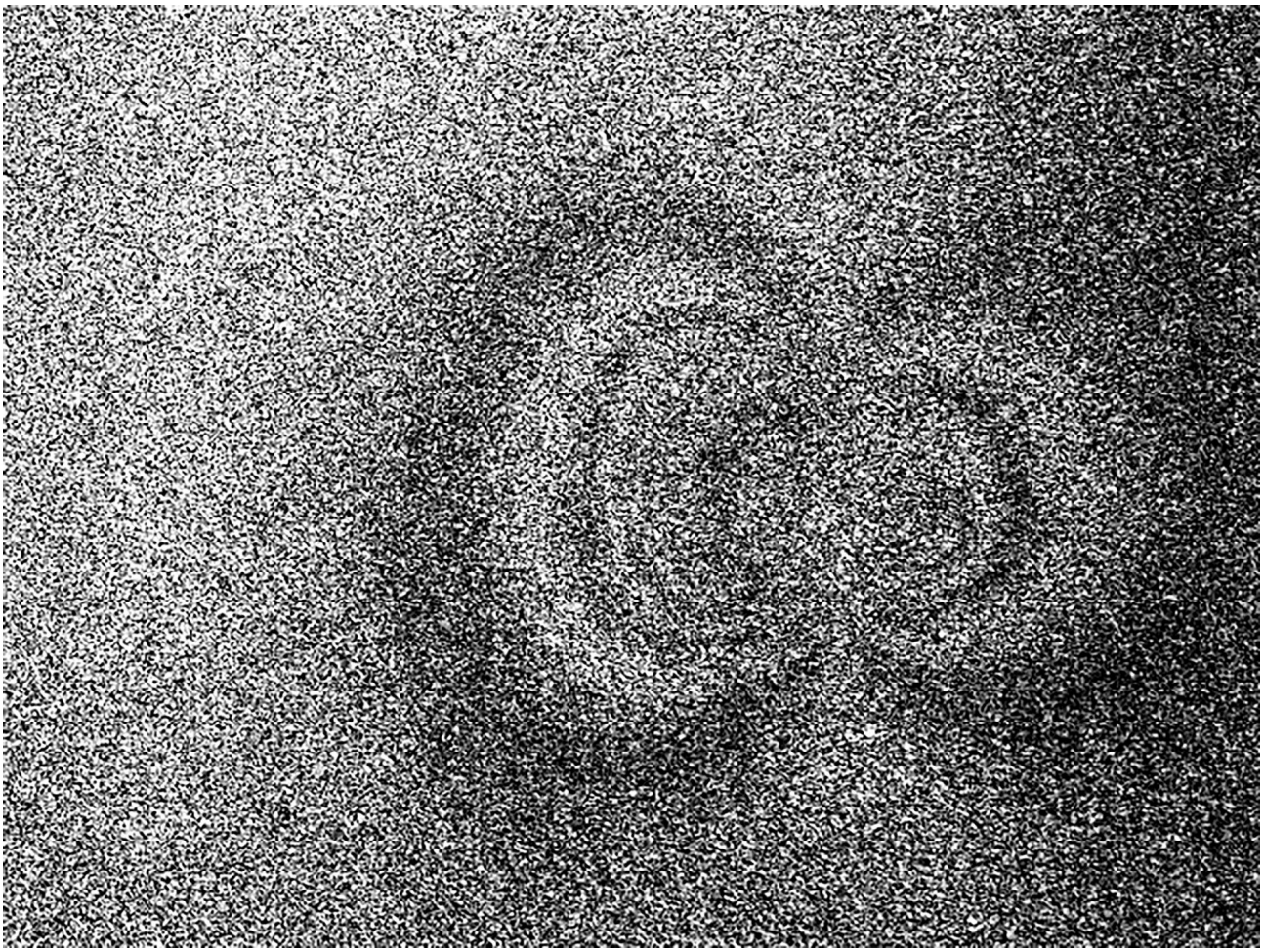

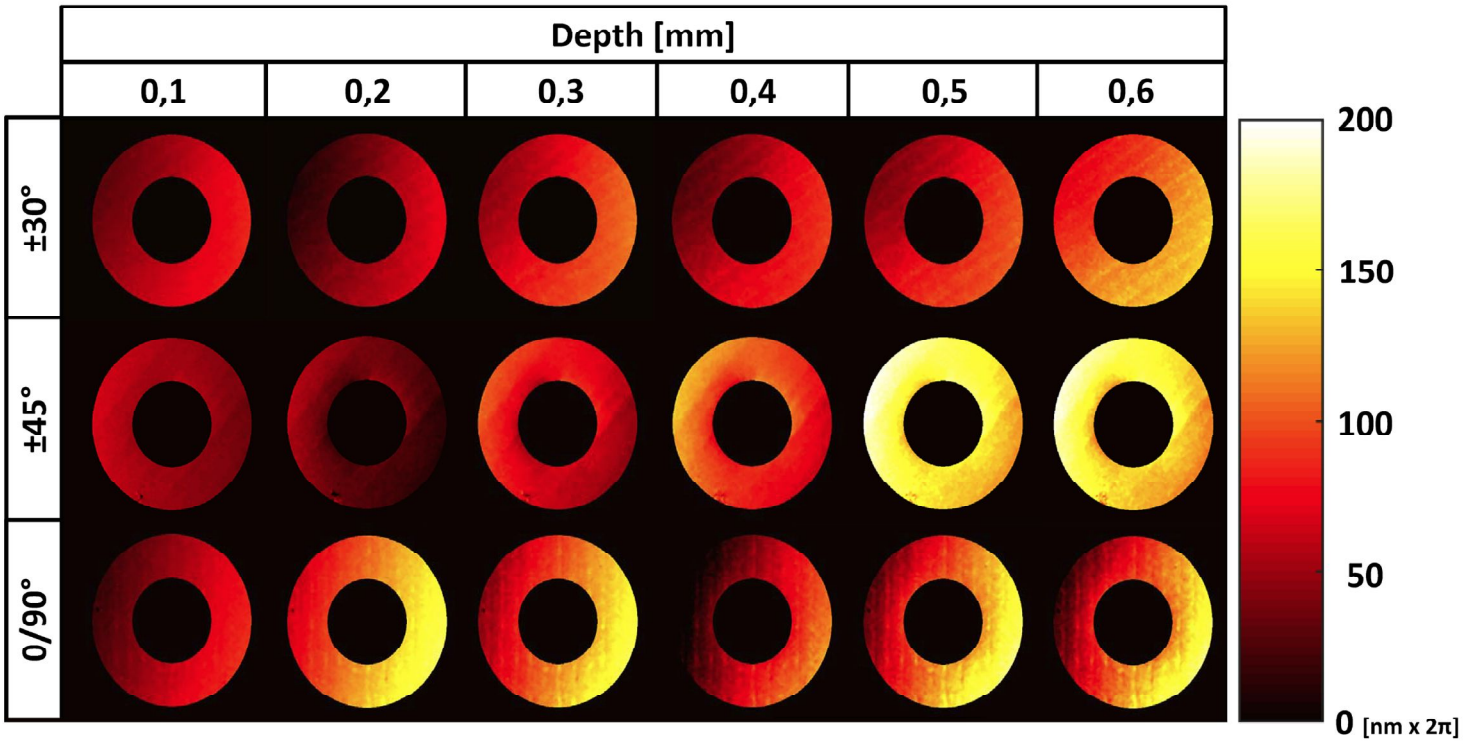
Depth [mm]
0,1
0,2
0,3
0,4
0,5
0,6
±30°
±45°
0/90°
200
150
100
50
0 [nm x 2π]

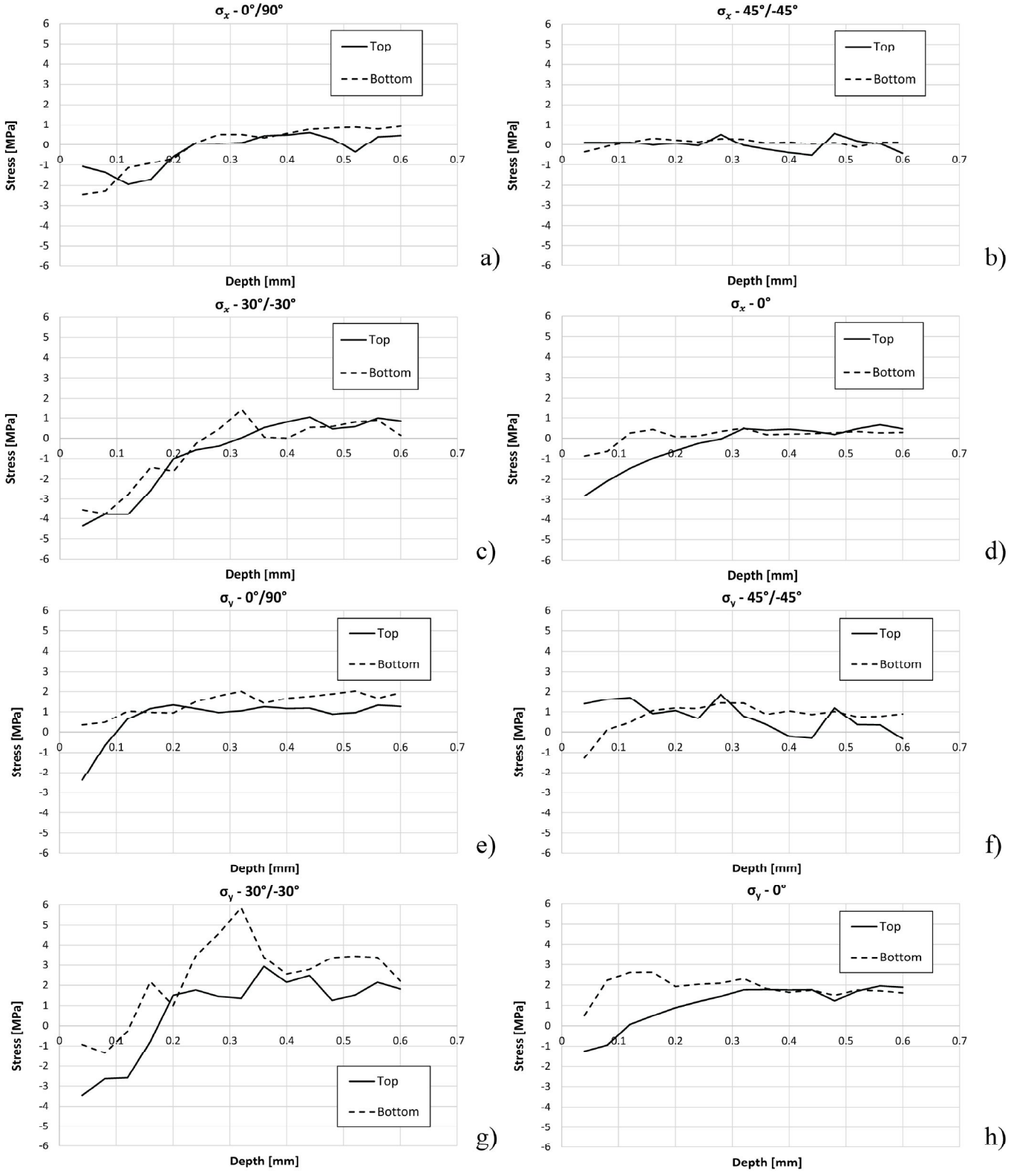
σx - 0°/90°
Top
Bottom
Stress [MPa]
Depth [mm]
a)
σx - 45°/-45°
Top
Bottom
Stress [MPa]
Depth [mm]
b)
σx - 30°/-30°
Top
Bottom
Stress [MPa]
Depth [mm]
c)
σx - 0°
Top
Bottom
Stress [MPa]
Depth [mm]
d)
σy - 0°/90°
Top
Bottom
Stress [MPa]
Depth [mm]
e)
σy - 45°/-45°
Top
Bottom
Stress [MPa]
Depth [mm]
f)
σy - 30°/-30°
Top
Bottom
Stress [MPa]
Depth [mm]
g)
σy - 0°
Top
Bottom
Stress [MPa]
Depth [mm]
h)

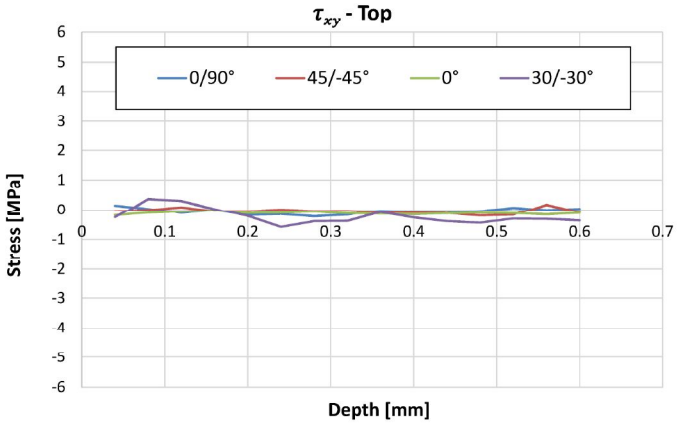
τ_{xy} - Top
0/90°
45/-45°
0°
30/-30°
Stress [MPa]
Depth [mm]

a)

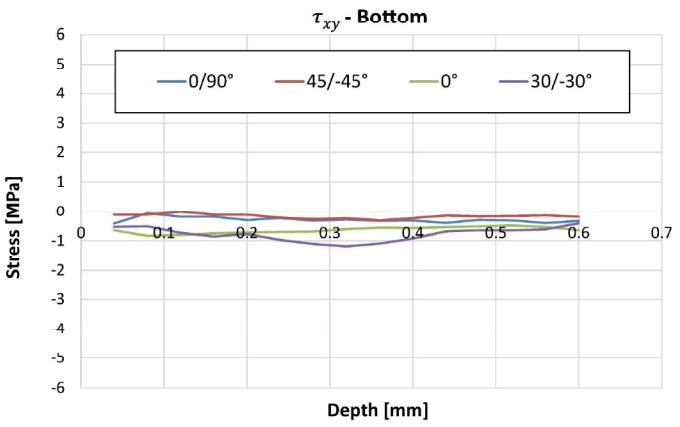
τ_{xy} - Bottom
0/90°
45/-45°
0°
30/-30°
Stress [MPa]
Depth [mm]

b)